2D Asymmetric Tensor Analysis

Xiaoqiang Zheng* Alex Pang†

Computer Science Department
University of California, Santa Cruz, CA 95064

ABSTRACT

Analysis of degenerate tensors is a fundamental step in finding the topological structures and separatrices in tensor fields. Previous work in this area have been limited to analyzing symmetric second order tensor fields. In this paper, we extend the topological analysis to 2D general (asymmetric) second order tensor fields. We show that it is not sufficient to define degeneracies based on eigenvalues alone, but one must also include the eigenvectors in the analysis. We also study the behavior of these eigenvectors as they cross from one topological region into another.

CR Categories: I.3.6 [Computer Graphics]: Methodology and Techniques—Interaction Techniques;

Keywords: critical points, general tensors, symmetric tensors, degenerate tensors, tensor topology, topological lines, hyperstreamlines,

1 INTRODUCTION

Many different physical processes can be described by 2nd order tensor fields. Two common examples are stress tensors in materials and geomechanics, and diffusion tensors in medical imaging. These types of tensors are generally symmetric tensors where there are no rotational components. For these, there are a few visualization techniques available such as tensor ellipsoids [9, 7], texture renderings [16, 6], volume rendering [8, 2, 14], and tensor topology [5, 13, 17]. However, there is a large class of mathematical and physical processes that cannot be adequately represented by symmetric tensors. This is particularly true in physical processes with strong rotational components such as general deformation tensors with both plastic and elastic deformations, and velocity gradient tensors in compressible flows. For these, there is a more limited set of tools available such as hyperstreamlines [3], and axis tripod glyphs [11].

The state of the art in visualizing general asymmetric tensor fields is to decompose them into a symmetric tensor field and a rotational vector field and then try to visualize these simultaneously or separately either continuously or with discrete glyphs [3, 11]. However, these approaches can hardly deliver the effect of the asymmetric tensor field as a whole entity. For example, the user has the daunting task of somehow integrating the rotational components depicted by ribbons along the major, medium and minor hyperstreamlines over the spatial domain of the data set.

The strategy proposed in this paper is to study the topology of asymmetric tensor fields directly without having to explicitly decompose them first. This paper will focus on the analysis and visualization of 2D general tensors of rank two.

*e-mail: zhengxq@cse.ucsc.edu
†e-mail:pang@cse.ucsc.edu

2 OVERVIEW

We classify a 2D general tensor as being in a real or a complex domain. If the tensor has all real eigenvalues, we say that it is in the real domain. If it has two complex eigenvalues, we say it is in the complex domain.

In general tensor fields, we also define a degenerate tensor as one with at least two repeated eigenvalues. Our investigations show that degenerate tensors in a typical asymmetric tensor field only have codimension one, rather than two as in symmetric tensors [17]. This means the degenerate features form *lines* in 2D tensor fields. In fact, we found the degenerate tensors form the *boundary* between the real and the complex domains.

Thus, unlike symmetric tensors, interpretation of the degenerate features is very different. That is, while the eigenvectors are indeterminate for double degenerate symmetric tensors, the same eigenvectors are determinate (and aligned) for double degenerate general tensors! Also note that in the real domain, the tensor has a stretching effect. While in the complex domain, the tensor has a swirling effect. This can be seen in Figure 1 which is the first such visualization of general tensor topology that we are aware of.

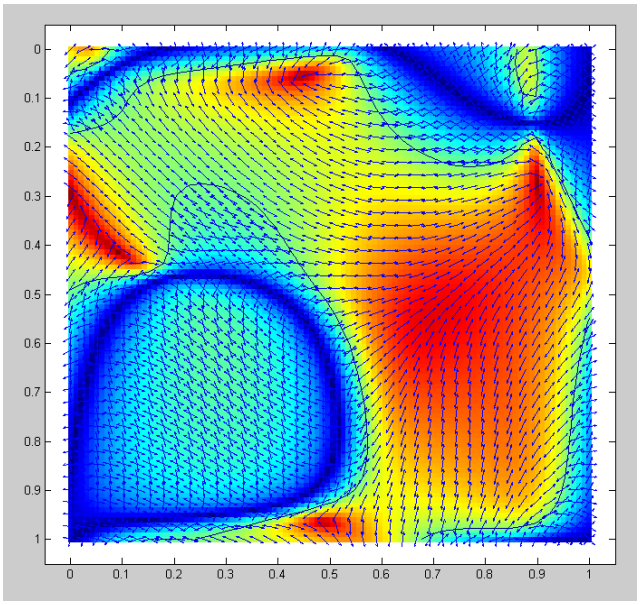

Figure 1: Composite vectors of a randomly generated asymmetric 2D tensor field. Warm color shows the complex domain and cool color shows the real domain. The tensors in the real domain are denoted by the two eigenvectors, while those in the complex domain are represented by the major dual-eigenvector J_1. The warmer the color, the closer the flow forms a perfectly circular path. The deep red regions are where the critical points can be found. The patterns appear to be similar to wedge and trisector points, but their behavior and interpretation are entirely different. The deep blue regions are where one can find symmetric tensors with no rotational components.

We notice that as we approach the degenerate lines from the real domain, the angle between the two eigenvectors got smaller and smaller. The two eigenvectors completely coalesce and do not form the full rank when they reach the degenerate boundary and cross into the complex domain. We can also show (see Section 4 that these degenerate lines are no longer the critical features in the topology of general tensor fields. Since the underlying data is smooth, the natural question is: What happens as we transition into the complex domain? How can we analyze and visualize the tensor and show the continuity of the data as we cross the boundary? Before we discuss this, we first review some previous work relevant to these questions.

3 Previous Work

In previous work on 2D tensor topology such as [4, 12], degeneracy in 2D symmetric tensors is defined as locations where there are repeated eigenvalues. Because the eigenvectors are indeterminate at these degenerate points, these are also the locations where hyperstreamlines may intersect.

Recall that for a 2D tensor T,

$$T = \begin{pmatrix} T_{00} & T_{01} \\ T_{10} & T_{11} \end{pmatrix} \tag{1}$$

the conditions for finding degenerate points in symmetric tensors are:

$$T_{00} = T_{11}, \qquad T_{01} = T_{10} = 0 \tag{2}$$

This work was extended to 3D symmetric tensor fields [5] where two types of degenerate points are identified: double degenerate points and triple degenerate points, where there are two and three repeated eigenvalues respectively. Subsequently, Zheng and Pang [17] pointed out that double degenerate tensors are stable features while triple degenerate points are not. Furthermore, double degenerate tensors form lines. More recent results [18] improved upon the original method of extracting double degeneracies using a more intuitive geometric formulation, and also using a tracing strategy based on the analytical tangents along the degenerate feature lines.

4 Composite Eigenvectors

In this section, we introduce a methodology to visualize and analyze an asymmetric tensor field in its entirety, without the need to decompose them into symmetric and rotational parts first. The advantage is that it focuses on the overall effect of the whole tensor field, and reflects the continuity of the tensors throughout different regions.

4.1 Dimensionality of Degenerate General Tensors

The definition of degenerate tensors in asymmetric tensor fields is still the same – repeated eigenvalues. This condition is equivalent to having the discriminant equal to zero. In a 3D symmetric tensor field, the discriminant $D_3(T)$ is always non-negative.

$$D_3(T) = (\lambda_1 - \lambda_2)^2(\lambda_2 - \lambda_3)^2(\lambda_3 - \lambda_1)^2 \tag{3}$$

Therefore, the degenerate tensors in a typical non-degenerate tensor field cannot form a surface. Otherwise, there will be a sign change between the two sides of the surface. But in a general tensor field, there is no constraint that the discriminant must be non-negative. The reason is that because the eigenvalues can be complex numbers, D_3 can be negative. This fact allows us to treat the discriminant as a scalar field and therefore, the degenerate tensors are simply the isosurfaces. Intuitively, the features should form surfaces. For degenerate 2D general tensors, the degenerate features is one dimension less and they form lines.

4.2 Eigenvectors and Degenerate Tensors

In a symmetric tensor field, a hyperstreamline is a streamline if we consider any group of the eigenvectors as regular vectors. The only places where these hyperstreamlines can intersect with each other are at the degenerate tensors, where the matrix has at least two repeated eigenvalues. This definition can be similarly extended into the asymmetric tensors. However, the degenerate tensor are curves rather than isolated points. It is not easy to naturally extend the concept of hyperstreamlines into visualizing such datasets, since the eigenvalues can be complex. Therefore it is natural to ask: What is the extension of hyperstreamlines into asymmetric tensor fields? Are degenerate tensors still the critical features?

For any 2D real asymmetric tensor, the two eigenvalues can either be two real or two complex conjugate eigenvalues. Therefore the tensor field is divided into the real and the complex domains. It is not difficult to develop techniques to analyze these two domains independently, but the key to a good method is to unite the visualization throughout the entire tensor field, since the data are continuous by its nature. From linear algebra, we know the quadratic discriminant of a 2D matrix is:

$$D_2 = (\lambda_1 - \lambda_2)^2 = (T_{11} - T_{22})^2 + 4T_{12}T_{21} \tag{4}$$

$D_2 > 0$ if the two eigenvalues are both real numbers, and $D_2 < 0$ if the two eigenvalues are conjugate conjugate numbers. When $D_2 = 0$, the two eigenvalues are equal. This result clearly points out that the boundary between the real and the complex domain are $D_2 = 0$, where the matrix has two repeated eigenvalues, i.e., a degenerate tensor.

When we start introducing the asymmetric part into a tensor field, not only do we change degenerate tensors into lines, but the role of degenerate tensors is significantly changed. In a symmetric tensor field, degenerate tensors are the critical feature where hyperstreamlines can intersect; in an asymmetric tensor field, degenerate tensors form the boundary between the real and the complex domain.

The eigenvectors around degenerate tensors also have significant changes. In a symmetric degenerate tensor, the eigenvectors associated with the repeated eigenvalues are indeterminate. Any vector in the plane spanned by two valid eigenvectors is another valid one. However, in an asymmetric degenerate tensor, the two eigenvectors completely overlap with each other, unless the tensor is symmetric, in which case, the eigenvectors are indeterminate. The eigenvector matrix do not span the full rank. In an asymmetric tensor field, if we approach the degenerate curve from the real side, we will see the two eigenvectors get closer and closer to each other. When they finally reach the boundary between the real and the complex domain, they completely overlap with each other. As we step into the complex domain, the data change smoothly even at the boundary between the real and the complex domain. So, the eigenvectors must change into another form that is still continuous with the coalesced eigenvectors at the boundary. The answer is the dual-eigenvector defined for an asymmetric tensor.

4.3 Dual-Eigenvectors

If a real matrix has a pair of complex conjugate eigenvalues, their associated eigenvectors E_1 and E_2 must also be complex conjugates. They are usually written as,

$$E_k = \overrightarrow{A} \pm i\overrightarrow{B}, k = 1, 2 \tag{5}$$

Therefore, the complex conjugate eigenvectors can be expressed by a pair of real vectors $(\overrightarrow{A}, \overrightarrow{B})$. However, such expression is not unique. If $\overrightarrow{A} \pm i\overrightarrow{B}$ is a pair of valid eigenvectors, then multiplying them with any complex number yields another valid pair.

$$\begin{aligned} & \overrightarrow{A}^* + i\overrightarrow{B}^* \\ = \; & (\cos(\alpha) + i\sin(\alpha))\,(\overrightarrow{A} + i\overrightarrow{B}) \\ = \; & \left(\cos(\alpha)\overrightarrow{A} - \sin(\alpha)\overrightarrow{B}\right) + i\left(\sin(\alpha)\overrightarrow{A} + \cos(\alpha)\overrightarrow{B}\right) \end{aligned} \tag{6}$$

In other words, if $(\overrightarrow{A}, \overrightarrow{B})$ is valid, then $(\overrightarrow{A}^*, \overrightarrow{B}^*) = \left(\left(\cos(\alpha)\overrightarrow{A} - \sin(\alpha)\overrightarrow{B}\right), \left(\sin(\alpha)\overrightarrow{A} + \cos(\alpha)\overrightarrow{B}\right)\right)$ is also valid for any α. So which $(\overrightarrow{A}^*, \overrightarrow{B}^*)$ is the most natural one? In this paper, we choose the $(\overrightarrow{A}^*, \overrightarrow{B}^*)$ that are perpendicular to each other, i.e., $\overrightarrow{A}^* \cdot \overrightarrow{B}^* = 0$. This leads to,

$$\begin{aligned} & \left(\cos(\alpha)\overrightarrow{A} - \sin(\alpha)\overrightarrow{B}\right) \cdot \left(\sin(\alpha)\overrightarrow{A} + \cos(\alpha)\overrightarrow{B}\right) = 0 \\ \Longrightarrow \quad & \overrightarrow{A} \cdot \overrightarrow{B}\tan(\alpha)^2 + \left(\|B\|^2 - \|A\|^2\right)\tan(\alpha) - \overrightarrow{A} \cdot \overrightarrow{B} = 0 \end{aligned} \tag{7}$$

Obviously, this quadratic equation have two distinct solutions in most cases. These two solutions are usually perpendicular to each other, which represents the two different ways to align them. To distinguish between these two solutions, we arbitrarily choose the one where $\|\overrightarrow{A}^*\| \geq \|\overrightarrow{B}^*\|$. For a pair of valid $(\overrightarrow{A}, \overrightarrow{B})$ that is also perpendicular to each other, we refer to the pair as the *natural basis* of the asymmetric tensor. However, when $\overrightarrow{A} \cdot \overrightarrow{B} = 0$ and $\|\overrightarrow{A}\| = \|\overrightarrow{B}\|$ hold at the same time, any real α yields a valid and natural basis. We refer to such points as *circular points*. This is similar to the degenerate symmetric tensor in that all vectors are valid eigenvectors. In fact, we can show later that such circular points are exactly the critical features of the topology of asymmetric tensor field. We are also going to show that the natural basis is closely related to the flow pattern contained in the Jacobian matrix around a critical point.

For a 2×2 matrix with two complex conjugate eigenvalues, we define its *dual-eigenvectors* as its natural basis $(\overrightarrow{A}, \overrightarrow{B})$. Since we usually choose $\|\overrightarrow{A}\| \geq \|\overrightarrow{B}\|$, $\overrightarrow{A}$ is referred as the *major dual-eigenvector* and $\overrightarrow{B}$ is referred as the *minor dual-eigenvector*.

4.4 Analysis of 2D Linear Flows

Here, we discuss some important properties of 2D linear flows and reveal its connection to dual-eigenvectors. Given a 2D tensor T as a Jacobian around a critical point, its trace is the rate of flow coming out of it. To concentrate on its flow property, we first make it traceless by removing the average away from its diagonal components, and calculate its deviator D_v. Then, we calculate its singular value decomposition (SVD): $D_v = U \cdot D \cdot V^T$, where U and V are two orthogonal matrices and D is a diagonal matrix with non-negative components. Without loss of generality, We define the two column vectors in U as J_1 and J_2. We choose them in such a way that their associated singular values of the deviator D_v satisfy: $\mu_1 \geq \mu_2$. Although this definition and calculation seems arbitrary, we can show that it has many interesting properties.

First of all, in the complex domain, the flow is either a swirling source or a swirling sink. That means the tendency is either to flow out or flow in. With the average of the diagonal components removed, the flow is completely closed. Any particle in this flow will follow a closed elliptical path. We can show that J_1 and J_2 are the long and the short axes of this ellipse, and the ratio between μ_2 and μ_1 represents its eccentricity. Therefore, they are a good representation of the flow in the complex domain. Most importantly, we can show $\left(\sqrt{\mu_1}J_1, \sqrt{\mu_2}J_2\right)$ form the natural basis of the asymmetric 2D tensor T. They are the simply the dual-eigenvectors after normalization.

Secondly, in the real domain, we can show that J_1 and J_2 are the angular bisectors of the true eigenvectors, E_1 and E_2, of T. That is why we call them dual-eigenvectors. Furthermore, J_1 equally bisects the smaller angle between E_1 and E_2, while J_2 bisects the larger angle between them. If we approach the degenerate curve from the real side, E_1 and E_2 get closer and closer to each other until finally, they also collapse into their angular bisector: J_1. Since the definition of J_1 is continuous across the degenerate lines, it means that the eigenvectors E_1 and E_2 in the real domain is continuous with the dual-eigenvector J_1.

4.5 Eigenvectors and Dual-Eigenvectors

We can prove that the relationship between the eigenvectors and the dual-eigenvectors, ignoring scaling, can be summarized as follows: In the real domain, $E_1 = \sqrt{\mu_1}J_1 + \sqrt{\mu_2}J_2, E_2 = \sqrt{\mu_1}J_1 - \sqrt{\mu_2}J_2$; and in the complex domain, $E_1 = \sqrt{\mu_1}J_1 + i\sqrt{\mu_2}J_2, E_2 = \sqrt{\mu_1}J_1 - i\sqrt{\mu_2}J_2$. These show that there is indeed a close relationship between the eigenvectors and their dual-eigenvectors. Therefore, we use the eigenvectors to represent the tensor in the real domain, and use the dual-eigenvectors to represent the tensor in the complex domain.

$$V_i(X) = \begin{cases} E_i, i \in \{1, 2\}, & \text{if T(X) is in real domain} \\ J_1, & \text{if T(X) is in complex domain} \end{cases} \tag{8}$$

From our analysis and Equation 8, we know V_1 and V_2 are both continuous vector fields. More importantly, they are also continuous through the boundary between the real and complex domains at the degenerate curves. Just as the topology of a symmetric tensor field is defined over its eigenvectors, we define the topology of a general tensor field over these composite vector fields V_1 and V_2. It is clear that the eigenvectors do not have critical feature in the real domain, exactly the reason why we choose the eigenvectors over the dual-eigenvectors in this case. We can show that the critical features of V_i are only found in the complex domain and are characterized as flows with perfectly circular path, i.e., they are the circular points given in the previous section. We can also show the criteria to find such points are as follows:

$$T_{00} = T_{11}, \qquad T_{01} + T_{10} = 0 \tag{9}$$

Since J_1 and J_2 are also the eigenvectors of $D_v D_v^T$, where D_v is the traceless deviator of T, the topological analysis around such critical features are also similar. The major dual-eigenvector J_1 also forms trisectors and wedges points. Although they come from very different definitions, it is interesting to compare this definition to the criterion of locating the degenerate points in a real symmetric tensor field,

$$T_{00} = T_{11}, \qquad T_{01} = T_{10} = 0 \tag{10}$$

From these two equations, it is easy to see that a degenerate symmetric tensor is automatically a circular tensor. The streamlines

following the composite eigenvectors can only intersect with each others at these circular points. This is very important in understanding the relationship between asymmetric and symmetric tensor field topology. If we start with a general tensor field and gradually reduce its anti-symmetric part, the critical features are contained in the complex domain. As the tensor field becomes more and more symmetric, the complex domain becomes smaller and smaller. But the critical points, i.e., the circular points, are still contained in such domains. Finally, the complex domains with the degenerate boundary and the circular points contained within the region shrink to individual degenerate points. The degenerate point can be considered as a "black hole" that eats up the old space and the "singularity".

4.6 Circular Discriminant

Equation 9 gives the criterion that we can use to identify the circular points in asymmetric tensor fields. In this section, we show that although our topological analysis on asymmetric tensor fields start with completely different origins, they have some very interesting connections with the established symmetric tensor topology.

If T is symmetric, Equation 2 can also be written as the quadratic discriminant as in Equation 4. D_2 is always non-negative for symmetric tensors. It equals to zero if and only if T is degenerate.

If T is asymmetric, we can define a similar scalar, *circular discriminant*, that is also non-negative all the time, but equals to zero if and only if T is a critical feature, i.e., the circular point.

$$\Delta_2 = (T_{11} - T_{22})^2 + (T_{12} + T_{21})^2 \tag{11}$$

We note that Δ_2 as defined in Equation 11, is rotational invariant for any 2×2 general matrix T. If T is in the real domain, then

$$\Delta_2 = \frac{(\lambda_1 - \lambda_2)^2}{\sin(\theta)^2} \tag{12}$$

where θ is the angle between the two eigenvectors E_1 and E_2. Such relationship clearly explains why the regular discriminant D_2 is equal to the circular discriminant Δ_2 when T is symmetric. This is because their only difference is the denominator $\sin(\theta)^2$, and θ is 90° for symmetric tensors. At first glance, Equation 12 seems to point out that Δ_2 would become zeros when $\lambda_1 = \lambda_2$. This conflicts with our previous conclusion that Δ_2 equals to zero only at the circular points, not the degenerate curves. This is because in an asymmetric tensor field, when $\lambda_1 = \lambda_2$, the two eigenvectors coalesce and therefore $\theta = 0$. This makes Equation 12 break down at the degenerate boundary curve. But, the equivalent Equation 11 still holds even at such places.

If T is in the complex domain, then

$$\Delta_2 = \frac{-(\lambda_1 - \lambda_2)^2}{\tan(\theta)^2} \tag{13}$$

Note that λ_1 and λ_2 are the complex conjugate eigenvalues, and the square of their difference has a negative sign. θ is defined as the angle between the two eigenvectors in its natural basis. $\tan(\theta/2) = \|B\|/\|A\|$. Similarly, Equation 13 also breaks down at the degenerate curves, but its limit when approaching this boundary can be computed through the equivalent Equation 11. It also points out Δ_2 is equal to zero when $\theta = 90^\circ$, which leads to $\|A\| = \|B\|$, i.e., the very definition of circular point.

5 Distance Measure For General Tensors

In this section, we propose a new scheme to measure the distance between two general matrices that are Jacobians of linear flow. Previous works such as earth mover's distance [10] used in flow feature comparisons only considered eigenvalues and ignored the information of the eigenvectors for 2D matrices. Not only is it difficult to extend the measure into 3D, but it is also possible to obtain a zero distance measure from two different flow patterns resulting in faulty comparison of flow features. Figure 2 shows several linear vector field that has zero earth mover's distance. From left to right, their Jacobians are $\begin{pmatrix} 1 & 0 \\ 0 & 1 \end{pmatrix}$, $\begin{pmatrix} 1 & 2 \\ 0 & 1 \end{pmatrix}$ and $\begin{pmatrix} 1 & -2 \\ 0 & 1 \end{pmatrix}$. These three Jacobians are all upper triangular matrices, therefore their eigenvalues are simply their diagonal components $(1, 1)$. Because their eigenvalues are the same, their distances are zeros and considered equivalent by earth mover's distance. But their visual difference can hardly be ingored.

Aside from feature comparisons, a properly justified distance measure is also useful in other situations. For example, Ye et al. [15] recently needed a distance measure between two Jacobian matrices of 3D flows in order to vary the seeding template used to generate streamlines.

One very important design property of such a distance measure is that it must be invariant to rotations. A matrix M_1 and itself after any orthogonal transformation is considered equivalent and their distance must be zero. If all such equivalent matrices form an object. A natural way to define the distance between two matrices is the distance between their equivalent group, i.e., their minimal distance after any rotations. For any two matrices M_1 and M_2, we have,

$$D(M_1, M_2) = \min_R \|M_1 - R^T M_2 R\|^2, \text{such that } R^T R = I \tag{14}$$

Note that such a distance automatically combines the eigenvectors into account and is independent of rotation as well. Any rotation on M_1 and M_2 does not change the distance measure $D(M_1, M_2)$ at all. To ignore the scaling effect, one can normalize M_1 and M_2 before computing their distance. The first order condition for an optimal R for an $N \times N$ general matrices is:

Theorem 5.1. *If M_1, M_2 is optimally aligned, then $[M_1^T, M_2]$ must be a symmetric matrix.*

where the notation $[A, B] = AB - BA$ is the commutator between the two matrices A and B. This theorem shows that the first-order condition for R to be optimal is that $[M_1^T, R^T M_2 R]$ is a symmetric matrix. A proof of this theorem is provided in the Appendix.

Solving such a system analytically for general $N \times N$ matrices is not simple. But it can be solved completely in some special cases. Two symmetric matrices S_1 and S_2 are said to be properly aligned if their eigenvectors are the same and the associated eigenvalues are ordered in the same way. Two general matrices M_1 and M_2 are said to be optimally aligned if $D(M_1, M_2) = \|M_1 - M_2\|^2$.

(1) For 2×2 general tensors, it can be shown that M_1 and M_2 are optimally aligned if their corresponding symmetric parts S_1 and S_2 are properly aligned.

(2) For $N \times N$ general tensors, if M_1 is symmetric, then M_1 and M_2 are optimally aligned if M_1 and the symmetric part of M_2, S_2, are properly aligned.

For matrices with a dimension higher than 2 and in its most general form, we may have to resort to numerical methods. In our experiments, a simple gradient descent or Newton-Raphson algorithm can achieve good convergence speed.

When dealing with 2×2 matrices, we need to add the following constraint to Equation 14: $det(R) = 1$. This makes the equivalent matrices limited to only the regular right hand coordinate system. With this additional constraint, we can differentiate left vortices from right vortices. Otherwise, with Equation 14 alone, the vector fields in Figure 2(b) and Figure 2(c) are considered the same. Note

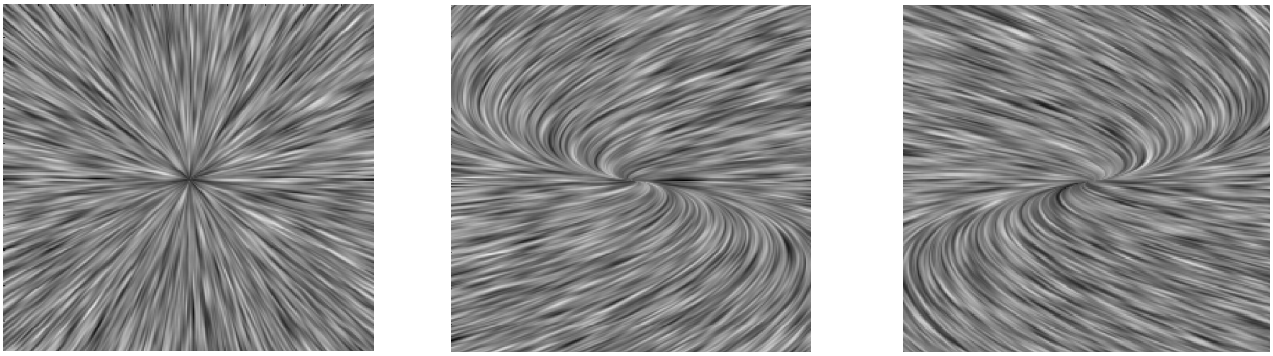

(a) Isotropic Sink (b) Clockwise Vortex (c) Counter-Clockwise Vortex

Figure 2: Three linear flow field that have the same eigenvalues. Therefore, the earth mover's distance between them are zeros.

that the need for the additional constraint only exists for matrices with even number of dimensions. For matrices with odd number of dimensions such as: 3×3 matrices, such constraint does not make any difference.

6 Implementation Issues

In this section, we discuss the computational issues with regards to obtaining the minimal distance between two Jacobian matrices.

6.1 Numerical Methods for Minimizing Distance

Equation 14 defines our distance to measure the difference between two Jacobian matrices. Due to the simplicity of this definition, it can be easily extended into higher dimensions. However, we can only solve this minimization problem analytical when (i) the matrices are 2×2; (ii) one of the matrices is symmetric.

For 3×3 Jacobians in 3D flow, we have to resort to numerical method. In our implementation, we use both gradient descent and the Newton-Raphson algorithm to iteratively update R. For the starting point, we choose R that properly aligns the symmetric parts of the two matrices M_1 and M_2. If the matrices are 2×2 or one of them is symmetric, such R can be proven to be optimal. In more general cases, we have to further update its values to the global minimum.

In this constrained optimization problem, our free variables are the three degrees of freedoms in choosing R. However, it is not simple to develop a stable iterative method based on implicit constraints. Our solution is to first parameterize R. There are many ways to represent an orthogonal matrix R. Here, we choose to represent $R = \exp(K)$ where K is an anti-symmetric matrix and $\exp$ is the matrix exponential [1]. It can be proven that this is equivalent to saying R is orthonormal. This property ensures that R is always in the neighborhood of I. An interesting property is of $\exp(K)$ in 3×3 cases is that it can be represented as a rotation around the axis $\overrightarrow{(K_{12}, K_{20}, K_{01})}$ for an angle of $\sqrt{K_{01}^2 + K_{12}^2 + K_{02}^2}$.

The second issue is to take first and second order derivatives of $D = \|M_1 - \exp(-K)M_{2,n}\exp(K)\|^2$ with respect to the three free variables in K at $K = 0$. Where $M_{2,n}$ is the nth iteration of M_2. This is tedious if we choose Euler angles as R's parameters. But it is very simple if we represent R in this matrix exponential form. Note that $\exp(K) = I + K + K^2/2 + O(K^3)$. we can also represent D as,

$$D = \|M_1 - (I - K + K^2/2)M_{2,n}(I + K + K^2/2) + O(K^3)\|^2 \quad (15)$$

It is much easier to evaluate different orders of gradients of D with respect to K in this form. After we obtain the new K using gradient descent or Newton-Raphson algorithm, we can easily get $R = \exp(K)$ using the formula for rotation along an axis. It is worth noting that we reset R to the identity matrix at every step, after assigning the previous R to M_2: $M_{2,n+1} = \exp(-K)M_{2,n}\exp(K)$ and $K = 0$. The Newton-Raphson version of this method usually converges within three to six iterations.

7 Results

In this section, we apply the techniques we introduced in this paper on several datasets.

We choose randomly generated tensor fields for its flexibility to generate many different datasets and great coverage of topological information. An asymmetric tensor is randomly generated at each grid point of a 4×4 coarse grid. Then, they are interpolated into a 30×30 fine grid using high-order interpolation to obtain a smooth data field. After this step, we use bilinear interpolation to obtain the tensor components within each cell.

Figure 3 shows results in such datasets using LIC to represent the composite eigenvectors. We choose two sets of tensor fields. For each set, we show the results from both the major and the minor composite eigenvectors. The colors are mapped to the distance of a tensor from being symmetric. The warmer the color, the more the flow pattern forms a circular path. The deep red is the critical feature of asymmetric tensor topology where we can find circular points. The deep blue regions are where we can find the symmetric tensors.

Note that for both the major and the minor composite eigenvectors, they are both continuous to the major dual-eigenvector at the degenerate curves. The major and the minor composite eigenvectors are the same within the complex domain, since they are both the major dual-eigenvectors in the complex domain. We can imagine that the minor dual-eigenvectors are on the axis that is perpendicular to the page. However, the major and the minor composite eigenvectors become more and more different when they are deeper into the real domain. When they reach the blue region i.e., the symmetric tensors, they are perpendicular to each other.

Figure 4 is a 3D multi-value multivariate data set. It covers a region from the Massachusetts Bay to the Cape Cod area off the U.S. East coast. Over 200 physical and bio-geochemical variables are measured. Forecasts and simulations were conducted for the period from August $17 - -$ October 5, 1998. The area of study in the Massachusetts Bay was divided into a 53×90 grid, and there are 600 values about each variable at each location in the grid. We examined a 2D slice of single realization of the flow velocity in this

data set, which we refer to as the `Massachusetts Bay` data set. Warmer colors in this figure corresponds to complex domains, which has more swirling behavior; cooler colors mean the real domain, which has more stretching behavior.

8 Conclusion and Future Work

In summary, the critical features in general tensor topology are not degenerate tensors any more, they are defined by the topology on the vector field V_1 and V_2, and characterized by Equation 9.

For 2D asymmetric tensor fields, our next task is to develop algorithms to extract the topology described above. The visualization should also encode information that are ignored above, such as the average of the diagonal components which shows whether the direction the particle is flowing in or out. We plan to get user evaluation and feedback from both flow and tensor communities.

Ultimately, we plan to extend this work to 3D general tensors. From the simple relationship between the eigenvectors and their dual-eigenvectors, it is possible to extend the ideas into 3D. But how to locate them in a numerically stable and efficient manner is still an open problem. Our research experience shows that it will be a very difficult problem. But the outcome is also very rewarding, since it automatically combines the flow features scientists and engineers are interested in from a general tensor field.

9 Acknowledgment

This work is supported by NSF ACI-9908881 and NASA Ames through contract # NAS2-03144 for the University Affiliated Research Center managed by the University of California, Santa Cruz under Task Order TO.035.0.DK.INR. We would like to thank Joel Yellin for discussions regarding commutators, singular perturbation theory, and quantum mechanics. Finally, thanks also go to Pierre Lermusiaux for the ocean circulation data set.

A Proof of Theorem 5.1

Theorem A.1. *If M_1, M_2 are optimally aligned, then $[M_1^T, M_2]$ must be a symmetric matrix.*

Proof. Let us consider all the paths of $R(t)$ such that $R(t)^T R(t) = I$ and $R(0) = I$. We know that the tangent space for orthogonal matrices at the identity matrix is the space of all the anti-symmetric matrices: $R'(0) = K$, where K can take the value of any anti-symmetric matrix. We define the distance between M_1 and $R^T M_2 R$ as,

$$\begin{aligned} D(t) = & \|M_1 - R^T M_2 R\|^2 \\ = & \text{tr}\left(\left(M_1^T - R^T M_2^T R\right)\left(M_1 - R^T M_2 R\right)\right) \\ = & \|M_1\|^2 + \|M_2\|^2 - 2\text{tr}\left(M_1^T R^T M_2 R\right) \end{aligned} \tag{16}$$

Define $F(t) = \text{tr}\left(M_1^T R^T M_2 R\right)$. It is obvious that the minimum of $D(t)$ is the maximum of $F(t)$. Therefore,

$$\begin{aligned} F'(0) = & \text{tr}\left(M_1^T R^T M_2 R\right)' \\ = & \text{tr}\left(M_1^T R'^T M_2 + M_1^T M_2 R'\right) \\ = & \text{tr}\left(M_1^T K^T M_2 + M_1^T M_2 K\right) \\ = & -\text{tr}\left(M_1^T K M_2\right) + \text{tr}\left(M_1^T M_2 K\right) \\ = & -\text{tr}\left(M_2 M_1^T K\right) + \text{tr}\left(M_1^T M_2 K\right) \\ = & \text{tr}\left(\left(M_1^T M_2 - M_2 M_1^T\right) K\right) \\ = & 0 \end{aligned} \tag{17}$$

Here we use the important property $\text{tr}(AB) = \text{tr}(BA)$. We define $H = [M_1^T M_2] = M_1^T M_2 - M_2 M_1^T$. Because M_1 and M_2 are optimally aligned, $F'(0) = \text{tr}(HK) = 0$ must hold for all anti-symmetric K.

$$\begin{aligned} F'(0) = & \text{tr}(HK) = \textstyle\sum_i (HK)_{ii} = \sum_{i,j} H_{ij} K_{ji} \\ = & \textstyle\sum_{i<j} (H_{ij} - H_{ji}) K_{ji} = 0 \end{aligned} \tag{18}$$

Since K_{ji} are all free variables, this implies that $H_{ij} - H_{ji} = 0$ must hold for all $i < j$. In other words, $H = [M_1^T, M_2] = M_1^T M_2 - M_2 M_1^T$ is a symmetric matrix.

□

References

[1] Marc Alexa. Linear combination of transformations. *ACM Transactions on Graphics*, 21(3):380–387, July 2002. Proceedings of ACM Siggraph 2002.

[2] A. Bhalerao and C.-F. Westin. Tensor splats: Visualising tensor fields by texture mapped volume rendering. In *Sixth International Conference on Medical Image Computing and Computer-Assisted Intervention (MICCAI'03)*, pages 294–901, Montreal, Canada, November 2003.

[3] T. Delmarcelle and L. Hesselink. Visualizing second-order tensor fields with hyperstreamlines. *IEEE Computer Graphics and Applications*, 13(4):25–33, July 1993.

[4] T. Delmarcelle and L. Hesselink. The topology of symmetric, second-order tensor fields. In *IEEE Visualization*, pages 140 –147, 1994.

[5] L. Hesselink, Y. Levy, and Y. Lavin. The topology of symmetric, second-order 3D tensor fields. *IEEE Transactions on Visualization and Computer Graphics*, 3(1):1–11, Jan-Mar 1997.

[6] I. Hotz, Z.X. Feng, H. Hagen, B. Hamann, K.I. Joy, and B. Jeremic. Physically based methods for tensor field visualization. In *Proceedings of Visualization '04*, pages 123–130, Austin, 2004.

[7] Gordon Kindlmann. Superquadric tensor glyph. In *Vissym'04*, pages 147–154, 2004. http://www.cs.utah.edu/~gk/papers/vissym04.

[8] Gordon L. Kindlmann and David M. Weinstein. Hue-balls and lit-tensors for direct volume rendering of diffusion tensor fields. In *IEEE Visualization*, pages 183–189, 1999.

[9] David Laidlaw, Eric Ahrens, David Kremers, Matthew Avalos, Russell Jacobs, and Carol Readhead. Visualizing diffusion tensor images of the mouse spinal cord. In *Proceedings of Visualization '98*, pages 127–134, 1998.

[10] Yingmei Lavin, Rajesh Batra, and Lambertus Hesselink. Feature comparisons of vector fields using earth mover's distance. In *Proceedings of Visualization '98*, pages 103–109, 524, October 1998.

[11] M. Livingston. Visualization of rotation fields. In *Proceedings of Visualization '97*, pages 491–494, 584, 1997.

[12] Xavier Tricoche, Gerik Scheuermann, and Hans Hagen. Scaling the topology of symmetric second order tensor fields. pages 171–184, 2003.

[13] Xavier Tricoche, Xiaoqiang Zheng, and Alex Pang. Visualizing the topology of symmetric, second-order, time-varying two-dimensional tensor fields. In J. Weickert and H. Hagen, editors, *Visualization and Image Processing of Tensor Fields*. Springer, 2005. Chapter 13.

[14] W.Benger and H.-C. Hege. Tensor splats. In *Visualization and Data Analysis*, pages 151–162, 2004.

[15] Xiaohong Ye and Alex Pang. Seeding strategies for 3d flow data. http://www.cse.ucsc.edu/research/avis/seed3d.html.

[16] Xiaoqiang Zheng and Alex Pang. HyperLIC. In *Proceedings of Visualization '03*, pages 249–256, Seattle, 2003.

[17] Xiaoqiang Zheng and Alex Pang. Topological lines in 3D tensor fields. In *Proceedings of Visualization '04*, pages 313–320, Austin, 2004.

[18] Xiaoqiang Zheng, Beresford Parlett, and Alex Pang. Topological lines in 3D tensor fields and discriminant hessian factorization. *IEEE Transactions on Visualization and Computer Graphics*, 2005. to appear.

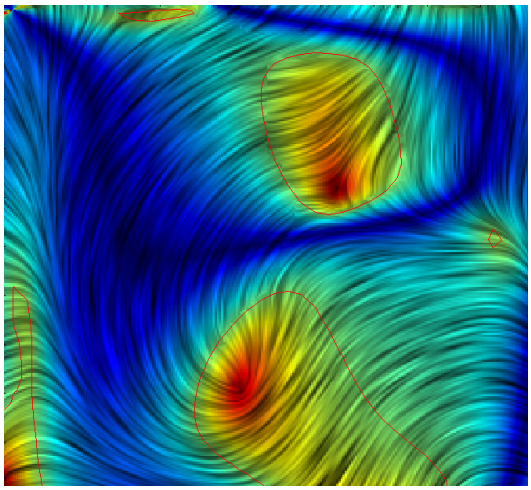

(a) First Set Major

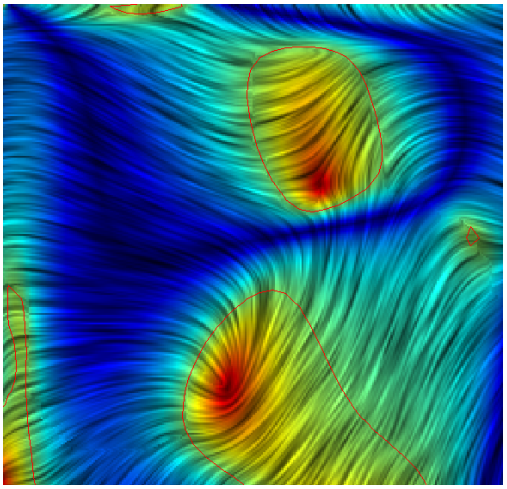

(b) First Set Minor

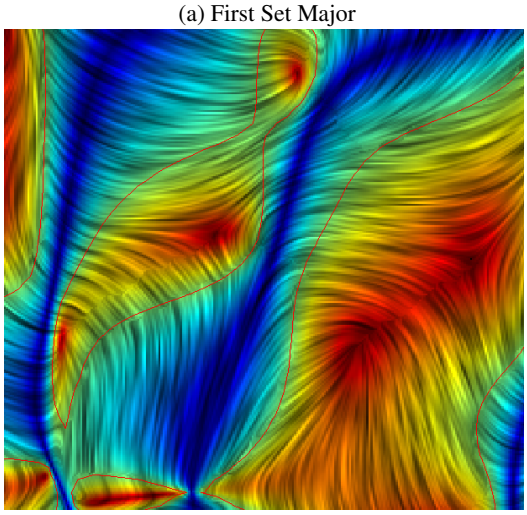

(c) Second Set Major

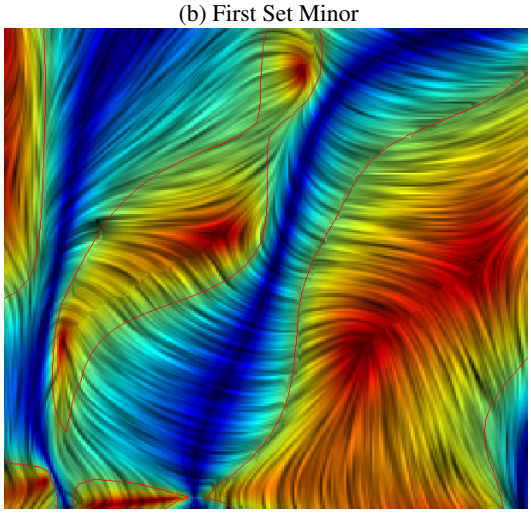

(d) Second Set Minor

Figure 3: Two sets of LIC images showing the composite eigenvectors of randomly generated asymmetric tensor fields.

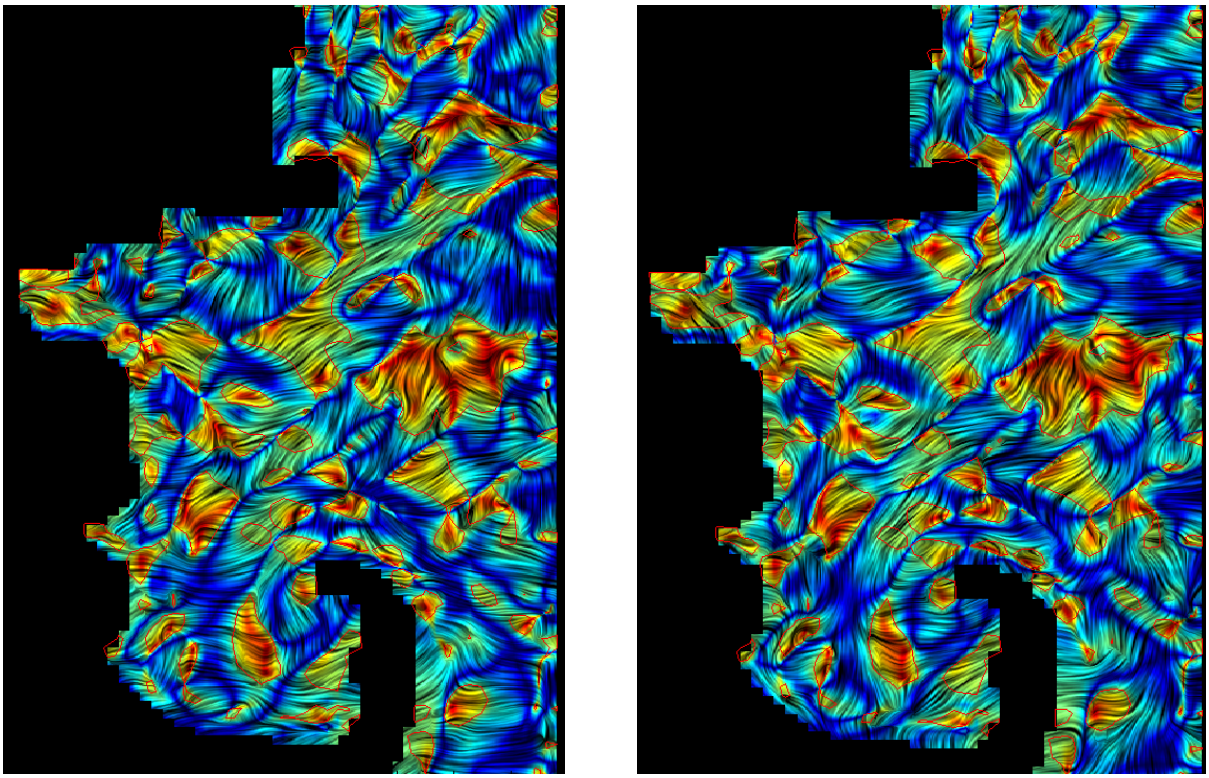

(a) Massachusetts Bay Major

(b) Massachusetts Bay Minor

Figure 4: Two sets of LIC images showing the composite eigenvectors of the Massachusetts Bay data set.